Localized states in the generalized Swift-Hohenberg equation

John Burke* and Edgar Knobloch
Department of Physics, University of California, Berkeley, California 94720, USA
(Received 15 December 2005; published 31 May 2006)

The Swift-Hohenberg equation with quadratic and cubic nonlinearities exhibits a remarkable wealth of stable spatially localized states. The presence of these states is related to a phenomenon called homoclinic snaking. Numerical computations are used to illustrate the changes in the localized solution as it grows in spatial extent and to determine the stability properties of the resulting states. The evolution of the localized states once they lose stability is illustrated using direct simulations in time.

I. INTRODUCTION

Ever since the observation that the subcritical complex Ginzburg-Landau equation exhibits stable spatially localized states [1] there has been considerable interest in the properties of these states. The presence of these states has important consequences for other systems described by partial differential equations on the line since the Ginzburg-Landau equation describes the behavior of such systems near bifurcation from the trivial state of the system. Specifically, the complex Ginzburg-Landau equation describes the evolution of a long wavelength oscillatory instability, as well as oscillatory instabilities at finite wavelength in systems with broken reflection symmetry. In contrast, near a steady state bifurcation with finite wavelength the evolution of the instability is described by the real Ginzburg-Landau equation, and this equation possesses only unstable spatially localized states. It is of interest therefore to examine what happens to these unstable states at larger amplitude, where the real Ginzburg-Landau equation no longer provides an adequate description of the system. In this paper we show that the localized states can become stable at such amplitudes, and indeed that there is a large multiplicity of coexisting stable localized states under very general conditions. We are able to relate the existence of these states to a phenomenon sometimes called *homoclinic snaking* that is well known from the theory of reversible systems with 1:1 resonance, and use this theory to construct a large number of such states. The stability properties of these states are also determined, and the evolution of nonstationary localized states is studied by numerical integration in time.

It is an interesting fact that closely related phenomena have already been described in several areas involving pattern formation. The theory was originally developed in the context of water waves, where localized states have been studied by moving into a reference frame of the waves and converting the problem into an ordinary differential equation (ODE). The resulting localized states are called solitary waves, and in some cases turn out to be solitons. Kirchgässner [2] has pioneered a successful approach to this type of problem that led to a number of advances in this area. Specifically, the ODE is viewed as a dynamical system in space,

and localized states are sought as homoclinic orbits connecting the trivial state to itself. Whether such orbits are possible depends in part on the stability properties of the trivial state: eigenvalues with positive real part indicate that a nontrivial state can grow from $x=-\infty$, while eigenvalues with negative real part indicate that such a state may return, under appropriate conditions, back to the trivial state as $x \rightarrow \infty$. The spectrum of the linearization about the trivial state is influenced by spatial symmetries of the system. In many cases, and in particular in the case considered here, the ODE is *reversible*. As a result the bifurcations that are encountered as a parameter is increased are nongeneric. In the present case the spatial dynamics of the system near the trivial state turn out to be described by the reversible 1:1 resonance. The unfolding of this resonance has been worked out in detail by Iooss and Perouème [3], and can be used to understand the appearance of a variety of homoclinic orbits in this system, and hence of localized states with different spatial structure.

Parallel to these developments Pomeau [4] presented an intuitive picture of why a multiplicity of localized states might be expected. In a typical (variational) system with bistability between two spatially homogeneous states all fronts connecting such states will move in such a way that the state of lower energy density invades the state of higher energy density; stationary fronts are present at isolated parameter values only, corresponding to equal energy densities (the Maxwell point). However, this is no longer so when a front connects a homogeneous state to a spatially periodic one, since the front can "lock" to the latter. The result is the presence of a pinning *region* in parameter space, straddling the Maxwell point, with localized states bounded by stationary fronts at either end. Some states of this type have been computed in subsequent work [5] on the Swift-Hohenberg equation with quadratic and cubic nonlinearities, and it is this work that provides the motivation for the present paper. We show here that multiple localized states are present in three distinct regions of parameter space, and relate their origin to the presence of reversible 1:1 resonances in the spatial dynamics of the system, thereby relating Pomeau's picture to subsequent mathematical developments, summarized in the physics literature by Coullet *et al.* [6], but anticipated by Champneys and colleagues in the context of localized buckling [7,8]. In fact Nishiura and Ueyama [9] identified the same type of behavior in a system of reaction-diffusion equations on the line in their study of self-replication. The latter paper has much in common with the

*Electronic address: burkej8@socrates.berkeley.edu

work of Hilali *et al.* [5] in the sense that it focuses on the dynamics that result from the depinning of the Pomeau fronts, without seeking a detailed explanation of the origin of the multiplicity of localized states.

With this brief (and incomplete!) overview we introduce in the next section the model system we study and summarize its basic properties. In Sec. III we discuss the so-called single pulse localized states in this system and describe their origin and stability properties; multipulse states are not considered. The range of existence of the single pulse states is explored in Sec. IV, followed by a concluding section that examines the relation of our results to earlier work by Hilali *et al.* and others, as well as to the mathematical theory alluded to above.

II. SWIFT-HOHENBERG EQUATION

We write the generalized Swift-Hohenberg equation in the form

$$\frac{\partial u}{\partial t} = ru - (\partial_x^2 + q_c^2)^2 u + vu^2 - gu^3 \tag{1}$$

used by Hilali *et al.* [5]. Here r is the control parameter while q_c, v and g are coefficients which we take to be $q_c=0.5$, $v=0.41$, $g=1$ as in Ref. [5]. In the presence of periodic boundary conditions with period L this equation possesses a Lyapunov functional F (which we refer to as an energy) given by

$$F = \int_0^L dx \left(-\frac{1}{2}ru^2 + \frac{1}{2}[(\partial_x^2 + q_c^2)u]^2 - \frac{1}{3}vu^3 + \frac{1}{4}gu^4 \right) \tag{2}$$

such that $\frac{\partial u}{\partial t} = -\frac{\delta F}{\delta u}$. It follows that along any trajectory the energy decreases to a (local) minimum. In particular no Hopf bifurcations are possible and (at fixed x) all time dependence ultimately dies out.

The linear stability of a stationary solution $u_s(x)$ of period L is determined by writing

$$u(x,t) = u_s(x) + \epsilon \tilde{u}(x)e^{\beta t}, \tag{3}$$

where β is the growth rate of the infinitesimal perturbation $\epsilon \tilde{u}(x)$. Thus $\tilde{u}(x)$ satisfies the eigenvalue problem

$$\beta \tilde{u}(x) = \mathcal{L}[u_s(x)]\tilde{u}(x), \quad \tilde{u}(x+L) = \tilde{u}(x), \tag{4}$$

where

$$\mathcal{L}[u_s(x)] \equiv [r - (\partial_x^2 + q_c^2)^2 + 2vu_s(x) - 3gu_s^2(x)] \tag{5}$$

is the linear differential operator obtained by linearizing the right side of Eq. (1) about $u_s(x)$, and the growth rate β is the associated eigenvalue.

A. Spatially homogeneous solutions

Flat, stationary solutions of Eq. (1) satisfy

$$0 = (r - q_c^4)u + vu^2 - gu^3. \tag{6}$$
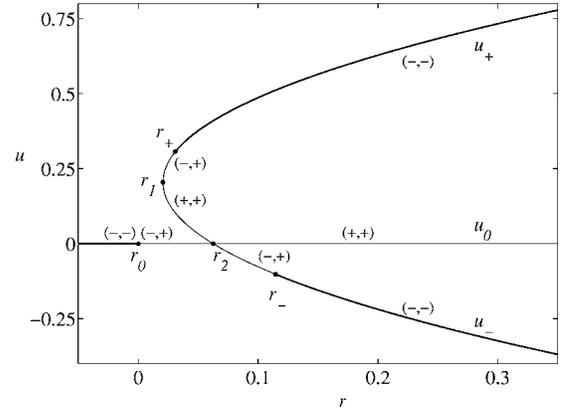
The three flat solution branches (shown in Fig. 1) are

FIG. 1. The flat stationary solutions u_0 and $u_\pm$ as a function of r. Stability with respect to uniform perturbations and perturbations with wave number q_c, respectively, is indicated by the signs of the corresponding eigenvalues. The labeled bifurcation points are $r_0 = 0$, $r_1 = 0.020\,475$, $r_2 = 0.0625$, $r_+ \simeq 0.030\,84$, $r_- \simeq 0.1146$.

$$u_0 = 0, \quad u_\pm = \frac{1}{2g}[v \pm \sqrt{v^2 + 4g(r - q_c^4)}]. \tag{7}$$

The $u_\pm$ branches are created in a saddle-node bifurcation at $r_1 \equiv q_c^4 - v^2/4g$. The u_- branches bifurcate from the trivial solution u_0 in a transcritical bifurcation at $r_2 \equiv q_c^4$.

For these states the eigenfunctions that solve Eq. (4) are $\tilde{u}(x) = \sin(kx)$, $\cos(kx)$. The corresponding growth rates on the u_0 and $u_\pm$ branches are

$$\beta_0 = r - (q_c^2 - k^2)^2, \tag{8a}$$

$$\beta_\pm = 3q_c^4 - (q_c^2 - k^2)^2 - 2r - \frac{v}{2g}[v \pm \sqrt{v^2 + 4g(r - q_c^4)}], \tag{8b}$$

respectively. For uniform states the domain size L used in Eq. (4) is arbitrary so these expressions are valid for all $k = 2\pi/L$. The u_0 branch is unstable to uniform perturbations ($k=0$) for $r > r_2$, while the $u_- > 0$ branch is unstable between the saddle-node bifurcation at r_1 and the transcritical bifurcation at r_2.

Increasing k up to q_c results in a monotonic increase in β, so at any fixed value of r the most unstable perturbations are those with wave number $k = q_c$. Increasing k also widens the domain of r over which the flat solutions are unstable. For each wave number k, the zeros of Eqs. (8a) and (8b) give the r values at which the branch first loses stability with respect to perturbations of wavelength $\lambda = 2\pi/k$:

$$r_{\lambda,0} = (q_c^2 - k^2)^2, \tag{9a}$$

$$r_{\lambda,\pm} = \frac{1}{2}\left(3q_c^4 - (q_c^2 - k^2)^2 \right.$$
$$\left. - \frac{v}{4g}\{v \pm \sqrt{v^2 + 8g[q_c^4 - (q_c^2 - k^2)^2]}\}\right). \tag{9b}$$

As a result the initial instability for all flat branches has wavelength $L_c = 2\pi/q_c$ and occurs at

$$r_0 \equiv r_{L_c,0} = 0, \qquad (10a)$$

$$r_\pm \equiv r_{L_c,\pm} = \frac{1}{2}\left[3q_c^4 - \frac{v}{4g}(v \pm \sqrt{v^2 + 8gq_c^4})\right]. \qquad (10b)$$

Further increase of k above q_c uniformly decreases the growth rate; for values of k above k_{max}, defined by

$$k_{max} = \left(q_c^2 + \sqrt{q_c^4 + \frac{v^2}{8g}}\right)^{1/2}, \qquad (11)$$

the growth rates $\beta_\pm$ are strictly negative and so the $u_\pm$ branches are stable to all short wavelength perturbations. The u_0 branch is only unstable to short wavelength instabilities at large values of r.

In the following we therefore focus on solutions to Eq. (1) with $L=L_c$, although at times it will be useful to take $L=nL_c$, with $n>1$ an integer.

B. Primary solutions with wavelength L_c and their stability

At the bifurcation points r_0 and $r_\pm$ branches of solutions with wavelength L_c are created. We compute the resulting branches of spatially periodic solutions using numerical continuation [10]. The results for the branch connecting the points r_0 and r_+, hereafter referred to as the "patterned" branch and denoted by u_P, are summarized in Fig. 2. Sample solution profiles are shown in Figs. 3(a) and 3(b). There are two Maxwell points of interest: at r_{M1} the patterned state has the same energy as the trivial flat state u_0, while at r_{M2} the patterned state has the same energy as u_+. Another branch of L_c-periodic states, created at r_- on u_-, extends all the way to $r=\infty$ but is omitted from the figure. In view of the symmetry $(v,u) \to (-v,-u)$ bifurcations from u_- with $v>0$ correspond to bifurcations from u_+ with $v<0$; such bifurcations from u_+ are also analyzed in what follows.

In addition we solve the eigenvalue problem (4) for the growth rate of perturbations with spatial period L_c. There is always (at least) one zero eigenvalue corresponding to the eigenfunction $\tilde{u}=du_s/dx$ generating infinitesimal translations. The remaining eigenvalues are determined numerically. The results for the patterned branch are summarized in Fig. 4. This branch is unstable near both ends but gains stability through saddle-node bifurcations at r_3 and r_4. All other eigenvalues (corresponding to eigenfunctions with wavelength L_c/m for integers $m \geq 2$) are negative, indicating that the patterned branch is stable with respect to short wavelength disturbances.

On larger domains the patterned states in Fig. 2(a) are subject to additional modes of instability. Figure 4(a) summarizes the resulting changes in stability while Fig. 4(b) shows the eigenvalues corresponding to eigenfunctions with wavelength $2L_c$. At the primary bifurcation points all the extra eigenvalues are negative. However, the eigenvalues of the two wavelength $2L_c$ eigenfunctions, which start at $\beta=-9q_c^4/16$ when $r=0$, change sign a total of four times, corresponding to four changes in stability of the patterned solutions with respect to wavelength $2L_c$ perturbations, and hence four secondary bifurcations to wavelength $2L_c$ solu-
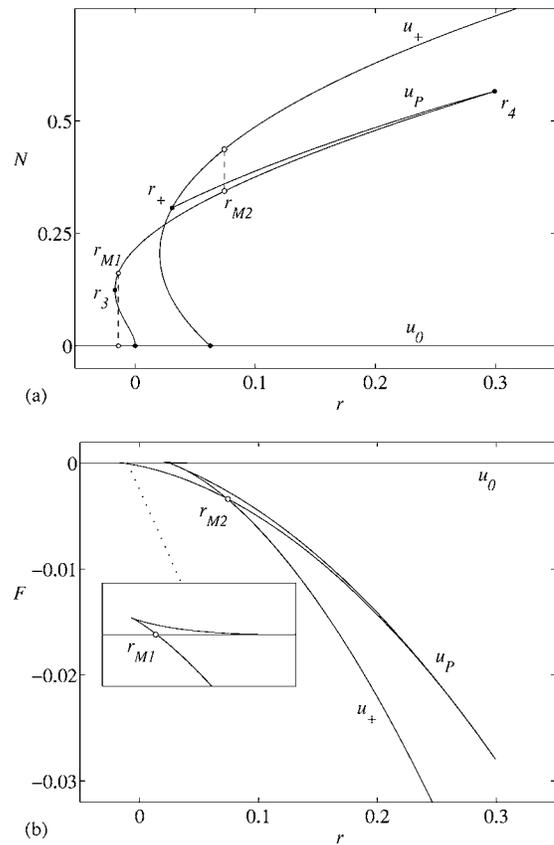

FIG. 2. (a) Bifurcation diagram showing the norm $N \equiv (L^{-1}\int_0^L u^2 dx)^{1/2}$ of the flat states with $u \geq 0$ and patterned states u_P with wavelength L_c as functions of r. The locations of the saddle nodes on the patterned branch are: $r_3 \simeq -0.016\,70$, $r_4 \simeq 0.2992$. (b) Energy F of the flat and patterned branches as a function of r; the inset shows an enlargement near $r=0$. The Maxwell points $r_{M1} \simeq -0.013\,81$ and $r_{M2} \simeq 0.073\,28$ are indicated in (a) by dashed vertical lines.

tions. Three of these crossings (labeled r_6, r_7, r_8) occur between r_+ and r_4 where the patterned branch is already unstable. The remaining bifurcation at r_5 reduces the stable domain of the patterned branch from $r_3 < r < r_4$ to $r_3 < r$
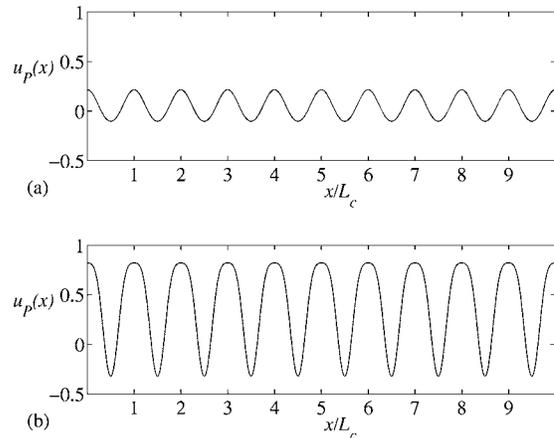

FIG. 3. Solution profiles $u_P(x)$ on the patterned branch. (a) $r \approx r_3$, (b) $r \approx r_4$.
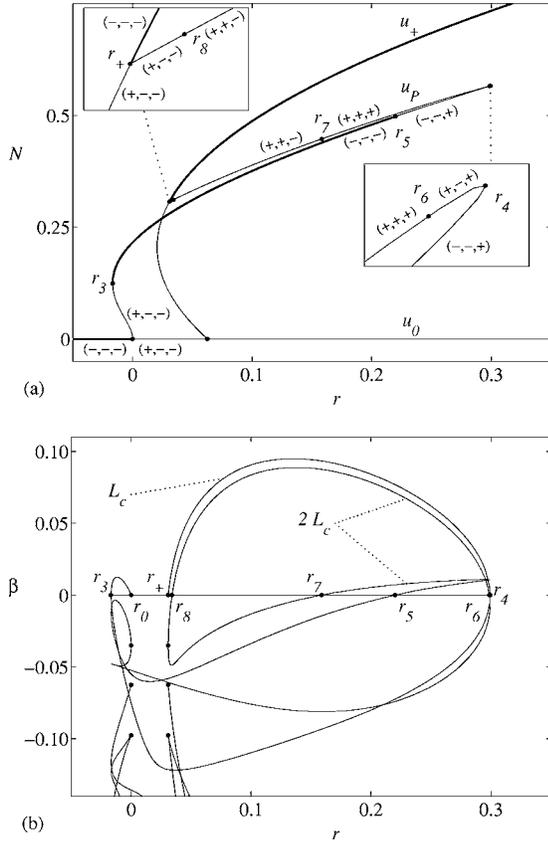
(a)

(b)

FIG. 4. (a) The stability of the patterned branch with respect to wavelength L_c and two different wavelength $2L_c$ modes, with – indicating stability and + instability. Thick lines indicate stable branches. The locations of the period-doubling bifurcations are $r_5 \simeq 0.2198$, $r_6 \simeq 0.2986$, $r_7 \simeq 0.1582$, $r_8 \simeq 0.03407$. (b) Growth rates on the patterned branch for perturbations of wavelength L_c and $2L_c$.

$< r_5$. Similar results hold for branches with spatial period nL_c, $n > 2$, although the number of distinct secondary branches grows quite rapidly, much as in other problems of this type [11]. The eigenvalues β corresponding to wavelength nL_c for integers $n = 1$, 2, 3, 4, and 5 are shown in Fig. 5. Observe that for each $n > 2$ there is at least one eigenvalue that passes through zero near r_5 (Fig. 5); this is so for larger values of n as well. A careful analysis of this region shows that although these bifurcations all occur at distinct values of r (invisible in Fig. 5) their location in r decreases as n increases. Based on detailed computations we surmise that as $n \to \infty$ these bifurcations accumulate at some $r = r_5^* \lesssim r_5$, with the result that the solutions along the patterned branch between r_3 and r_5^* are stable to *all* long wavelength perturbations. Thus the "bifurcation" at which the patterned states lose stability with increasing r is in fact a much more complicated object than implied in Ref. [5]. Similar clustering of eigenvalues has been observed in other problems of this type [9], but to the authors' knowledge the reason for this behavior remains unclear.

III. LOCALIZED STATES

With the above background we turn to the study of spatially localized states. The first class of localized solutions of
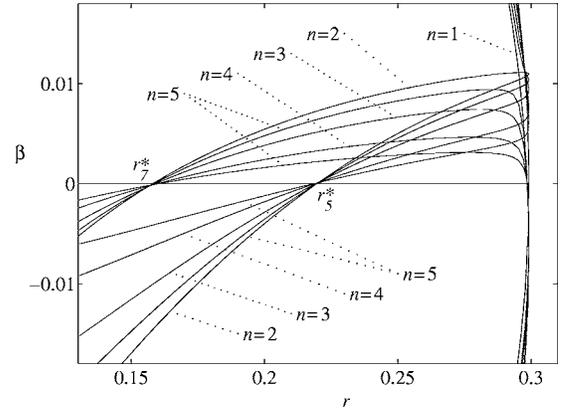

FIG. 5. The growth rate β on the patterned branch of perturbations of wavelength nL_c for $n = 1$, 2, 3, 4, and 5. As $n \to \infty$ the individual bifurcations accumulate at r_5^* and r_7^* (see text).

interest are small amplitude stationary states biasymptotic to u_0, which exist near $r = 0$. The time-independent version of Eq. (1) forms a fourth order reversible dynamical system in space: the equation is invariant under the spatial reflection $(x \to -x, u \to u)$. Any localized state connecting to the trivial state $u_0 = 0$ as $x \to \pm\infty$ requires that u_0 has both stable and unstable spatial eigenvalues. It is easy to check that for $r < 0$ these eigenvalues are $\pm iq_c \pm (\sqrt{-r/2q_c}) + O(r)$, while for $r > 0$ they are $\pm iq_c \pm i(\sqrt{r/2q_c}) + O(r)$. Thus for $r < 0$ the eigenvalues form a quartet, and u_0 is hyperbolic with two stable eigenvalues and two unstable eigenvalues. In contrast for $r > 0$ all the eigenvalues lie on the imaginary axis and u_0 is not hyperbolic. In particular it is not possible to approach u_0 as soon as $r > 0$; thus no localized states can be present when $r > 0$ [12]. At $r = 0$ there is a pair of imaginary eigenvalues $\pm iq_c$ of double multiplicity. The bifurcation at $r = 0$ is thus a Hopf bifurcation in a reversible system with 1:1 resonance [3]. Theory shows that under certain conditions the hyperbolic regime ($r < 0$, $|r| \ll 1$) contains a large variety of spatially localized states.

Two of these states can be constructed using perturbation theory. We define the small parameter ϵ by $r = -\epsilon^2 \mu_2$, $\mu_2 > 0$, and look for stationary solutions of Eq. (1) of the form

$$u_s(x) = \epsilon u_1(x,X) + \epsilon^2 u_2(x,X) + \cdots, \tag{12}$$

where $X \equiv \epsilon x$ is a large scale over which the amplitude of the pattern changes. It follows that

$$u_1(x,X) = Z_1(X)e^{iq_c x} + \mathrm{c.c.}, \tag{13a}$$

$$u_2(x,X) = \frac{2v}{q_c^4}|Z_1|^2 + \frac{v}{9q_c^4}Z_1^2 e^{2iq_c x} + Z_2(X)e^{iq_c x} + \mathrm{c.c.} \tag{13b}$$

The amplitude $Z(X,\epsilon) \equiv Z_1(X) + \epsilon Z_2(X) + \cdots$ satisfies the equation

$$4q_c^2 Z_{XX} = \mu_2 Z - \gamma_3 Z|Z|^2 + \frac{i\epsilon}{q_c}\left(-\frac{32v^2}{27q_c^4}Z_X|Z|^2 + 4q_c^2 Z_{XXX}\right)$$

$$+ \frac{\epsilon^2}{q_c^2}\left(\frac{8v^2}{q_c^4}Z(|Z|^2)_{XX} + \frac{28v^2}{27q_c^4}Z^*(Z^2)_{XX} + \gamma_5 Z|Z|^4\right.$$

$$\left. + q_c^2 Z_{XXXX}\right) + O(\mu_2\epsilon^2, \epsilon^3). \qquad (14)$$

Here

$$\gamma_3 = \frac{38v^2}{9q_c^4} - 3g, \quad \gamma_5 = -\frac{3g^2}{64q_c^2} + \frac{5795gv^2}{144q_c^6} - \frac{3521v^4}{432q_c^{10}}.$$

Since $\gamma_3 \simeq 8.35 > 0$ the bifurcation at the origin is *subcritical*. This asymptotic result is formally valid only in the limit $\epsilon \to 0$ although some of the higher order terms have been kept for later reference.

The simplest nontrivial solution of Eq. (14) is the uniform solution

$$Z(X) = (\mu_2/\gamma_3)^{1/2}e^{i\phi} + O(\epsilon), \qquad (15)$$

corresponding to spatially periodic states with period L_c near $r=0$, viz.

$$u_P(x) = 2\left(\frac{-r}{\gamma_3}\right)^{1/2}\cos(q_c x + \phi) + O(r). \qquad (16)$$

Here ϕ is an arbitrary phase and $\mu_2 > 0$ (so $r<0$). Other solutions to Eq. (14) can be found in terms of elliptic functions, and localized states correspond to infinite period solutions of this type with $Z \to$ as $X \to \pm\infty$:

$$Z(X) = \left(\frac{2\mu_2}{\gamma_3}\right)^{1/2}\text{sech}\left(\frac{X\sqrt{\mu_2}}{2q_c}\right)e^{i\phi} + O(\epsilon). \qquad (17)$$

This solution corresponds to

$$u_\ell(x) = 2\left(\frac{-2r}{\gamma_3}\right)^{1/2}\text{sech}\left(\frac{x\sqrt{-r}}{2q_c}\right)\cos(q_c x + \phi) + O(r). \qquad (18)$$

Like the spatially periodic states this family of solutions is parametrized by $\phi \in S^1$, which controls the phase of the pattern within the sech envelope. Within the asymptotics this phase remains arbitrary; there is no locking between the envelope and the underlying wave train at any finite order in ϵ. However, it is known [13–15] that this is no longer the case once terms beyond all orders are included. These terms break the rotational invariance of the envelope solution and result in a weak flow on the circle S^1. This flow in turn *selects* specific values of the phase: $\phi=0$ and $\phi=\pi$ [16]; since S^1 is a circle one of these must be weakly attracting and the other weakly repelling, cf. Fig. 10 below. At the same time these terms lead to transversal crossing of stable and unstable manifolds of u_0 [6] thereby producing the snaking that becomes so prominent farther away from $r=0$. Note that the phases $\phi=0, \pi$ are the only two phases that preserve the symmetry ($x \to -x$, $u \to u$). It follows that *two* branches of
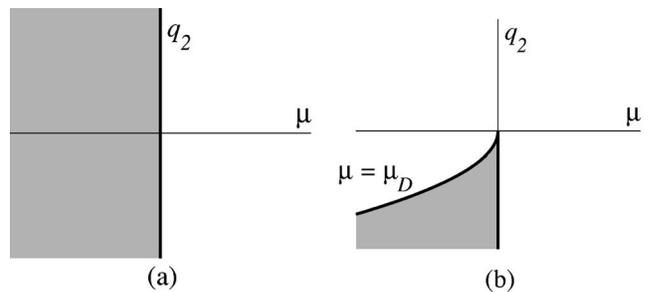

FIG. 6. For (a) $q_4 < 0$ and (b) $q_4 > 0$ the normal form contains homoclinic orbits to the trivial state when the parameters μ and q_2 fall within the shaded region. The solid line $\mu = \mu_D$ in (b) marks the location of heteroclinic orbits between the trivial state and a nontrivial state.

localized states bifurcate subcritically from $r=0$, one of which is stable with respect to translations of the envelope relative to the wave train, the other being unstable. Both states are amplitude-unstable [17]. Near $r=0$ these two branches are essentially indistinguishable, but one might expect that with increasing $-r$ the differences will grow and therefore that two distinct branches will emerge from $r=0$.

To prove that the localized states calculated above exist in a finite neighborhood of the origin we analyze the stationary solutions of Eq. (1) near the bifurcation at the origin using normal form theory. The appropriate normal form for the reversible Hopf bifurcation with 1:1 resonance is [3]

$$A' = iq_c A + B + iAP\left(\mu; |A|^2, \frac{i}{2}(AB^* - A^*B)\right), \qquad (19a)$$

$$B' = iq_c B + iBP\left(\mu; |A|^2, \frac{i}{2}(AB^* - A^*B)\right)$$

$$+ AQ\left(\mu; |A|^2, \frac{i}{2}(AB^* - A^*B)\right), \qquad (19b)$$

where in the context of spatial dynamics the prime denotes differentiation with respect to x, the functions A and B transform under spatial reflection as $(A,B) \to (A^*, -B^*)$, and P and Q are polynomials with real coefficients which to lowest order take the form

$$P(\mu; y, w) = p_1\mu + p_2 y + p_3 w, \qquad (20a)$$

$$Q(\mu; y, w) = -q_1\mu + q_2 y + q_3 w + q_4 y^2. \qquad (20b)$$

The bifurcation from the trivial state occurs at $\mu=0$, and this state is hyperbolic in the region $\mu<0$ provided $q_1>0$. The fact that the normal form is completely integrable [3] is of great assistance in its analysis. One finds that there are two possible types of behavior depending on the sign of q_4 at $q_2=0$. When $q_4<0$ homoclinic solutions are present in the whole half space $\mu<0$ [Fig. 6(a)]. In contrast, when $q_4>0$ homoclinic solutions are present only for $q_2<0$ and then only between $\mu_D < \mu < 0$, where $\mu_D = -3q_2^2/16q_1q_4$ [Fig. 6(b)]. At μ_D homoclinic solutions terminate in a heteroclinic connection between the flat state ($A=0$) and a nontrivial state ($A \neq 0$) with the same energy.

It should be noted that for $\mu = -\epsilon^2\mu_2 < 0$, where $\mu_2 = O(1)$, we can introduce a large spatial scale $X \equiv \epsilon x$. The transformation $(A, B) = (\epsilon \tilde{A}(X), \epsilon^2 \tilde{B}(X))e^{iq_c x}$ permits us to eliminate $\tilde{B}$ from the normal form, resulting in

$$A'' = q_1\mu_2 A + q_2 A|A|^2 + \frac{i\epsilon}{2}[-4p_1\mu_2 A' + (6p_2 - q_3)A'|A|^2$$

$$+ (2p_2 + q_3)A^2(A^*)'] + \epsilon^2\{p_3[A^*A' - A(A^*)']A'$$

$$+ (q_4 - q_3p_2 + p_2^2)A|A|^4\} + O(\mu_2\epsilon^2, \epsilon^3), \quad (21)$$

where the prime now denotes derivatives with respect to X and we have dropped the tildes.

A comparison of this equation with Eq. (14) permits us to identify the coefficients in the normal form in terms of the parameters of the Swift-Hohenberg equation. To transform Eq. (14) into the same form as Eq. (21) we note that it is possible to remove all second and higher order derivatives up to any order in ϵ by iteratively replacing Z_{XX} with its power series expansion. Introducing the nonlinear transformation $Z = A + \epsilon^2\rho A|A|^2$ allows matching at $\mu_2 = 0$ through order ϵ^2, and subsequent unfolding allows matching of the μ_2 terms up to order ϵ. The results are [18]

$$p_1 = -\frac{1}{8q_c^3}, \quad q_1 = \frac{1}{4q_c^2}, \quad \rho = -\frac{9g}{16q_c^4} + \frac{355v^2}{216q_c^8}, \quad (22a)$$

$$p_2 = \frac{9g}{16q_c^3} - \frac{187v^2}{216q_c^7}, \quad q_2 = \frac{3g}{4q_c^2} - \frac{19v^2}{18q_c^6} = -\frac{\gamma_3}{4q_c^2},$$
$$(22b)$$

$$p_3 = -\frac{8v^2}{9q_c^8}, \quad q_3 = \frac{3g}{8q_c^3} - \frac{41v^2}{108q_c^7}, \quad (22c)$$

and

$$q_4 = -\frac{177g^2}{128q_c^6} + \frac{5089gv^2}{288q_c^{10}} - \frac{78131v^4}{7776q_c^{14}}. \quad (22d)$$

Matching at higher orders in ϵ involves higher order terms omitted from the expansion (20) of the polynomials P, Q. The above results can also be obtained through a lengthier calculation of the explicit reversibility-preserving normal form transformations at $r = 0$, followed by appropriate unfolding.

For the parameter values used here $q_2 < 0$, corresponding to the *subcritical* case [3]. As q_2 is not small, q_4 does not play an important role in classifying the dynamics, and both Figs. 6(a) and 6(b) predict that homoclinic connections to the $A = 0$ state are present for $\mu < 0$. These are precisely the states calculated explicitly in Eq. (18). However, the scaling assumed in Eq. (12) fails for small q_2 and the localized structures then take a different form [19].

In the following we use the continuation package Hom-Cont to extend the solutions (18) with $\phi = 0, \pi$ to solutions of Eq. (1) valid farther away from $r = 0$. Technically the numerical routine finds reflection symmetric solutions to Eq. (1) on a large but finite domain L, but provided the width of the resulting localized state is smaller than the domain (typically
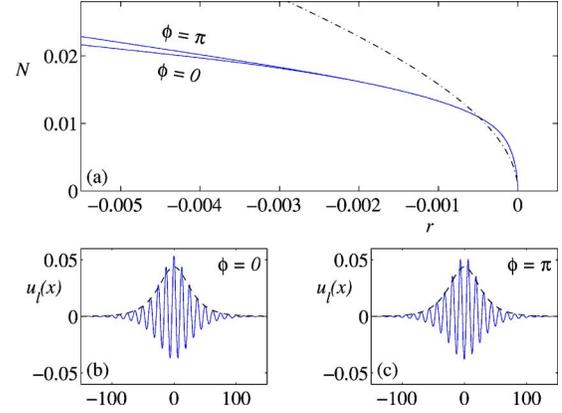

FIG. 7. (Color online) (a) Bifurcation diagram showing the $\phi = 0$ and $\phi = \pi$ branches of homoclinic states near $r = 0$. The branch of uniform patterned solutions (dot-dash) is also shown. The vertical axis is the norm N taken over a large but finite domain in x. The lower panels show the homoclinic solutions $u_\ell(x)$ on the (b) $\phi = 0$ and (c) $\phi = \pi$ branches at $r = -0.002$. The dashed lines in these panels show the leading order envelope computed in Eq. (18).

$40L_c$) the true homoclinic connection is well approximated by a large period orbit. Figure 7 illustrates some of the results obtained in this manner for small $-r$ while Fig. 8 extends these results to larger values of $-r$. Sample profiles along each branch are shown in Fig. 9. Along the $\phi = 0$ branch the midpoint ($x = 0$) of the localized state is always a local maximum, while along the $\phi = \pi$ branch the midpoint is always a local minimum. Near the origin the amplitude is small and the width of the sech envelope is large enough to contain many wavelengths of the underlying pattern. Away from the origin the amplitude grows and becomes comparable to the amplitude of the patterned states (specifically, the stable branch beyond the bifurcation at r_3) and the width
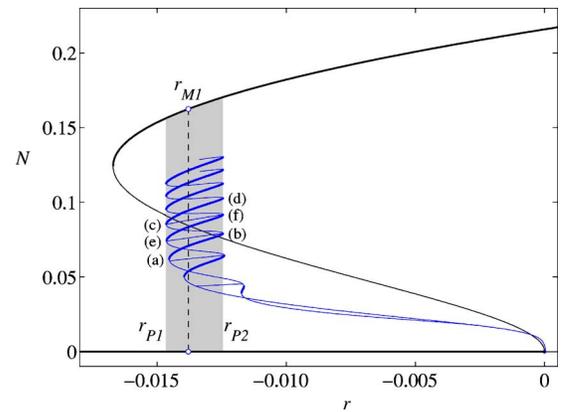

FIG. 8. (Color online) Bifurcation diagram showing the two homoclinic branches together with the flat and patterned branches of Fig. 4. Away from the origin the homoclinic branches are contained within the pinning region (shaded) between $r_{P1} \simeq -0.01464$ and $r_{P2} \simeq -0.01245$, and are then linked by secondary branches of localized but asymmetric states. Thick lines indicate stable solutions. The dashed vertical line marks the location of the Maxwell point r_{M1} between the flat and patterned branches. The letters (a)–(f) mark the locations of the profiles shown in Fig. 9.
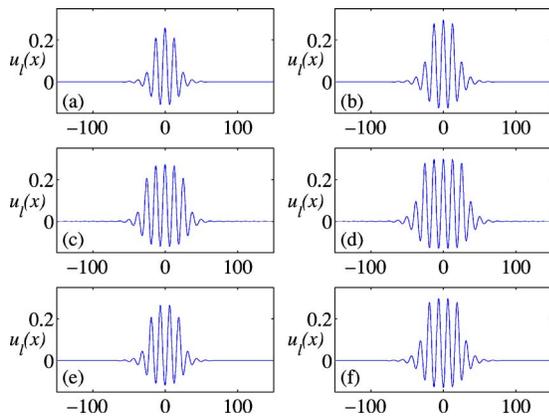
FIG. 9. (Color online) Sample profiles $u_\ell(x)$ at the saddle-nodes indicated in Fig. 8. (a)–(d) lie on the $\phi=0$ branch while (e) and (f) lie on the $\phi=\pi$ branch.

decreases until it is comparable to L_c, the wavelength of the underlying pattern. Beyond this point both the $\phi=0$ and $\phi=\pi$ branches undergo a series of saddle-node bifurcations responsible for the terminology *homoclinic snaking*. Each saddle-node bifurcation adds a pair of oscillations to the profile $u_\ell(x)$, and the saddle-node bifurcations asymptote exponentially rapidly to r_{P1} and r_{P2}. At each value of r within this range there exists an infinite number of solutions, each of a different width. Higher up along each "snake" the solutions $u_\ell(x)$ begin to look like a pattern of wavelength L_c and uniform amplitude, truncated at either end by a stationary "front" of width of order L_c connecting this state to u_0. The amplitude of this state is nearly identical to the upper branch of the patterned solutions. These results suggest that within the region $r_{P1} < r < r_{P2}$ there exist *heteroclinic* connections between the flat and patterned states as well. Far up each branch shown in Fig. 8, after many saddle-node bifurcations, the homoclinic solutions $u_\ell(x)$ connecting the flat state u_0 to itself resemble two of these heteroclinic connections, from u_0 up to the patterned state and then from the patterned state back down to u_0. We identify these states with the Pomeau fronts; as in his scenario these fronts are stationary because of pinning by the underlying wave train. Indeed we may think of the region $r_{P1} < r < r_{P2}$ as a Maxwell point that has been broadened by pinning to the underlying patterned state, a picture supported by the presence within this region of the Maxwell point r_{M1} at which the u_0 and patterned branches have the same energy.

Figure 8 also indicates the stability of the localized solutions in time, a consideration that is absent from the general theory of reversible systems. The eigenvalue problem (4) yields the growth rate of infinitesimal perturbations of the homoclinic solutions at each point along the branches, as well as the associated eigenfunctions $\tilde{u}(x)$. The latter are localized around the base state $u_\ell(x)$ and are therefore insensitive to the exact choice for L. The results for the $\phi=0$ and $\phi=\pi$ branches are shown in Fig. 10. This analysis confirms that both branches are unstable near the origin. The $\phi=\pi$ branch [Fig. 10(b)] has two positive eigenvalues. Of the corresponding unstable modes one is even in x and corresponds to an amplitude perturbation of the small sechlike solution.
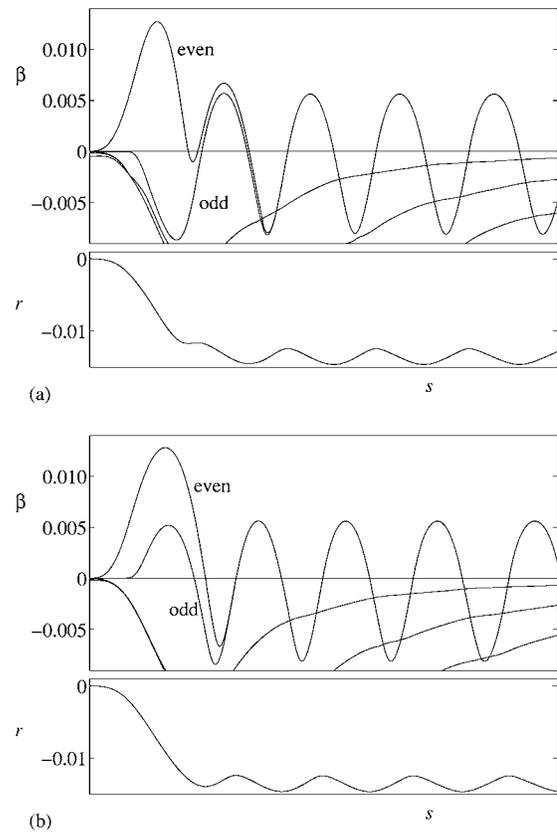

FIG. 10. Spectrum of growth rates β on the (a) $\phi=0$ and (b) $\phi=\pi$ branches homoclinic to the $u_0=0$ flat state as a function of the arc length s along the branch measured from the bifurcation at the origin (upper panels). The lower panels show the corresponding branches as a function of s.

The other is odd and corresponds to a phase perturbation that pushes the envelope away from $\phi=\pi$. The $\phi=0$ branch [Fig. 10(a)] has only one positive eigenvalue corresponding to an even amplitude perturbation. On both branches the phase eigenvalues remain almost zero until the snakes develop. Once this happens the stability is controlled by a single even mode and a single odd mode—several other modes approach zero growth rate but never cross. Each crossing of the even mode corresponds to a saddle-node bifurcation in Fig. 8. The crossings of the odd mode correspond to bifurcations to branches of asymmetric solutions that form "rungs" linking the $\phi=0$ and $\phi=\pi$ branches, a few of which are shown in Fig. 8, cf. Ref. [20]. After the first few folds the two eigenvalues approach one another rapidly, indicating that the symmetry-breaking bifurcations approach the saddle-node bifurcations. When this happens the eigenfunctions become localized around the two fronts while preserving their parity (Fig. 11). It follows that there are *stable* homoclinic solutions of arbitrary width along both the $\phi=0$ and $\phi=\pi$ branches. The *heteroclinic* connections are therefore also stable, as hypothesized by Pomeau.

Although the snaking of the true homoclinic orbit represented in Fig. 8 goes on forever, the solutions shown in the figure were found on a finite domain in x. In these circumstances the sequence of saddle-node bifurcations must terminate: as the domain fills with the pattern the snakes terminate
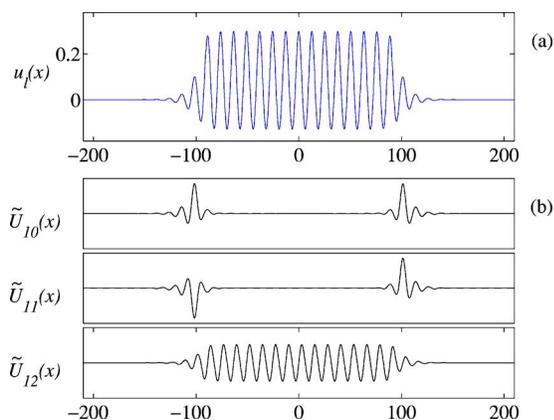
FIG. 11. (Color online) (a) Solution profile $u_\ell(x)$ at r_{P2} high up the $\phi=0$ snaking branch. (b) The three eigenfunctions of interest. The corresponding eigenvalues (growth rates) are all zero at r_{P2}. Away from the saddle node the eigenvalues of the first two are nonzero but the general shape and symmetry remains.
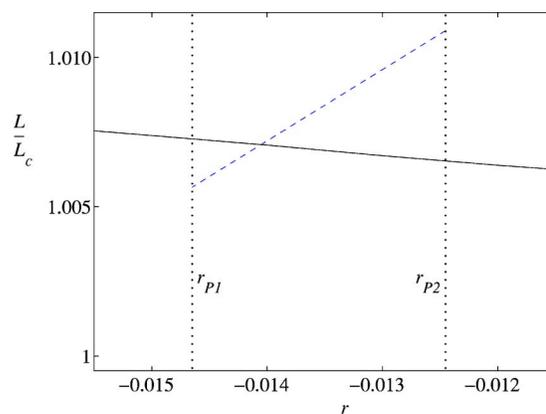

FIG. 12. (Color online) Plot of the wavelength of the pattern within the localized states (dashed line) found in the pinning region between r_{P1} and r_{P2}, and the preferred wavelength of the stable uniform patterned solution based on energy minimization (solid line).

on the patterned branch. The termination point corresponds to a bifurcation at which a pair of homoclinic branches biasymptotic to the *patterned state* is created, similar to the bifurcation at the other end of the snake at $r=0$. This duality is a generic feature in problems of this type [21]. Numerical analysis beyond that presented here indicates that the location of this bifurcation coincides with the saddle-node bifurcation at r_3.

A. Wavelength selection

Close examination of the wide homoclinic solutions (far up the snakes) shows that despite appearances the shape inside the envelope does not match the patterned branch perfectly. The largest deviation is in the wavelength, which is typically slightly larger than L_c. Near the bifurcations at r_0 and r_+ there exists a continuum of bifurcations to branches of solutions with wavelengths near L_c. These branches look qualitatively similar to the wavelength L_c branch shown in Fig. 2. Perturbations with wavelength L_c are always the most dangerous instability for the flat states, and near such bifurcations the wavelength L_c branches are energetically favored over branches with other wavelengths. At large amplitude this is no longer the case, however, and on large domains we may expect the preferred solution to shift from this wavelength. Figure 12 shows the wavelength of the preferred solution in the neighborhood of the pinning region. This curve was found by minimizing the energy density of the solutions with respect to the spatial period L, at fixed r. Figure 12 also shows the wavelength of the pattern within the localized states. Far up the snaking branch, where the localized state contains many wavelengths of the pattern, this wavelength is spatially uniform and independent of the width of the localized state. It is not independent of r, however. Pomeau's pinning mechanism allows for the existence of localized states away from the Maxwell point, but evidently the wavelength of the patterned domain within such states is affected by the presence of the fronts at either side: near r_{P1}, where the flat state is energetically favored, the packet is squeezed

tighter, while near r_{P2}, where the patterned state is favored, the packet expands. This is a frustration effect: the fronts at $r_{P1} < r < r_{M1}$ want to move in such a way as to eliminate the localized state, leading to a compression of the state relative to its wavelength at the Maxwell point $r=r_{M1}$ (Fig. 12). Likewise at $r_{M1} < r < r_{P2}$ the fronts want to move outwards, thereby stretching the localized state. It is noteworthy that the resulting compression or expansion is distributed uniformly across the localized state, a fact that appears to be a consequence of local energy minimization. As a consequence the localized states approach a *different* spatially periodic state at each r, although in Fig. 8 (as well as later bifurcation diagrams) we use the wavelength L_c patterned branch as a stand-in for the actual periodic state approached by the snaking. Some aspects of wave-number selection at moderate amplitude can be captured using improved perturbation theory [19].

B. Depinning transition

The discussion summarized above indicates that below r_{P1} the (heteroclinic) fronts connecting the flat and patterned states are no longer stationary, and will instead drift in such a way that the patterned state is gradually eliminated until the lower energy flat state fills the entire domain. Above r_{P2} the fronts also cease to be stationary but now drift in such a way as to expand the patterned state until it fills the whole domain. Likewise the stationary homoclinic states that are present everywhere within the pinning region also cease to be stationary, and evolve to either the flat or patterned state. A homoclinic localized state like those shown in Fig. 8 but at a small distance outside the pinning region (for example, at $r=r_{P2}+\delta$, with $\delta \ll 1$,) will evolve slowly at first because of its proximity to the saddle-node bifurcation. As it evolves farther away from the saddle node its shape will change more rapidly, its width increasing abruptly by one wavelength on either side (or decreasing, if $r=r_{P1}-\delta$), until it approaches the neighborhood of the next saddle-node bifurcation. Since the saddle nodes almost line up (Fig. 13) the profile will
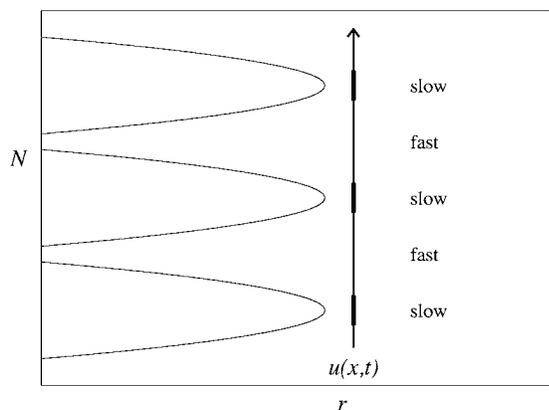
FIG. 13. Schematic representation of the evolution of a time-dependent state just outside the pinning region.

grow in a sequence of quick "bursts" as it passes between the saddle nodes (or shrink, as it passes the ones at r_{P1}). These bursts can be viewed as *nucleation* events. An example of this evolution is shown in Fig. 14 in the form of a space-time plot.

The transition time T to pass between two consecutive saddle nodes follows from a semianalytic analysis of the dynamics near the bifurcation [22]. We let $U_0(x)$ be the stationary localized state at the depinning transition $\delta=0$. For $|\delta| \ll 1$ we then have $u(x,t) = U_0(x) + |\delta|^{1/2} u_1(x,t) + \cdots$, at least while the solution remains near $U_0(x)$. It follows that $u_1(x,t)$ satisfies the equation

$$\mathcal{L}u_1 = \partial_t u_1 - |\delta|^{1/2} [\mathrm{sgn}(\delta) U_0 + v u_1^2 - 3g U_0 u_1^2] + O(|\delta|),$$
(23)

where $\mathcal{L} = \mathcal{L}[U_0]$ is the linearized Swift-Hohenberg operator (5) at r_{P2}. This equation must be solved subject to the requirement that $|u_1| \to 0$ as $|x| \to \infty$. Since for $|\delta| \ll 1$ the perturbation u_1 evolves on the timescale $|\delta|^{-1/2}$ the right hand side of this equation is uniformly small. Thus at leading or-
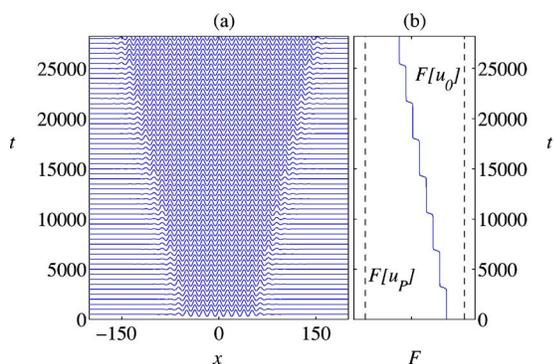

FIG. 14. (Color online) (a) Time evolution of a localized state outside the pinning region, at $r \simeq r_{P2} + 7 \times 10^{-5}$. The width increases symmetrically in a series of abrupt steps separated by nearly stationary episodes that last for $T \simeq 3500$. (b) The steps are seen more easily in a plot of the energy $F(t)$. The dashed vertical lines mark the energy density corresponding to a domain filled with the flat ($F[u_0]=0$) or patterned ($F[u_P] \simeq -1.88 \times 10^{-5}$) state.

der we solve $\mathcal{L}u_1 = 0$, i.e., the eigenvalue problem (4) restricted to the $\beta=0$ subspace. At a saddle node high up each snake $U_0(x)$ has a three-dimensional neutral eigenspace spanned by $\tilde{U}_{10}(x)$ (the even mode whose eigenvalue vanishes at the saddle node), $\tilde{U}_{11}(x)$ (the odd mode that tracks the even mode ever more closely as one moves up the snakes), and $\tilde{U}_{12}(x)$ [the neutrally stable odd mode $U_0'(x)$]. Sample profiles of these eigenfunctions can be seen in Fig. 11 taken at one of the saddle nodes at r_{P2} located far up the snake, corresponding to a wide localized state. It follows that

$$u_1(x,t) = a(t)\tilde{U}_{10}(x) + b(t)\tilde{U}_{11}(x) + c(t)\tilde{U}_{12}(x) + O(|\delta|^{1/2}),$$

where $a(t)$, $b(t)$, and $c(t)$ are slowly evolving real amplitudes. The evolution equations for these amplitudes are obtained by imposing solvability conditions on Eq. (23); since $\mathcal{L}$ is self-adjoint this condition requires that the right hand side be orthogonal to all null eigenvectors. The resulting calculation can be simplified by noting that in the space of reflection-symmetric perturbations the "center of mass" of the pattern remains fixed. Consequently we may set $b \equiv c \equiv 0$, leaving (cf. Ref. [22])

$$\alpha_1 \dot{a} = |\delta|^{1/2} [\alpha_2 \mathrm{sgn}(\delta) + \alpha_3 a^2] + O(|\delta|),$$
(24)

where

$$\alpha_1 \equiv \int_{-\infty}^{\infty} \tilde{U}_{10}^2 dx \simeq 0.2564,$$
(25a)

$$\alpha_2 \equiv \int_{-\infty}^{\infty} U_0 \tilde{U}_{10} dx \simeq 0.2036,$$
(25b)

$$\alpha_3 \equiv \int_{-\infty}^{\infty} (v - 3g U_0) \tilde{U}_{10}^3 dx \simeq 4.558 \times 10^{-3}.$$
(25c)

The integrals have been evaluated using numerically generated values for $U_0(x)$ and $\tilde{U}_{10}(x)$ at the saddle node at r_{P2}. As α_2 and α_3 are of the same sign there are two solution branches present in $\delta < 0$ while for $\delta > 0$ the solution runs away, consistent with the location of r_{P2} on the right side of the line of saddle nodes. The transition time T to pass between successive saddle nodes is estimated as the time it takes the solution of Eq. (24) to pass from $-\infty$ to $+\infty$, viz.

$$T = \frac{\pi \alpha_1}{(|\delta| \alpha_2 \alpha_3)^{1/2}} \simeq \frac{26.44}{|\delta|^{1/2}}.$$
(26)

Figure 15 shows the transition times, determined through explicit time integration of the type shown in Fig. 14, for several values of r near r_{P2}. The predicted value (26) compares well with the best fit to the data: $T \simeq 24.90 |\delta|^{-1/2}$. It should be noted that an identical calculation applies near r_{P1}, except that here α_2 and α_3 are of opposite signs.

C. Other types of localized states

The localized states of the previous section were found in a region of bistability, bounded on one side by the bifurca-
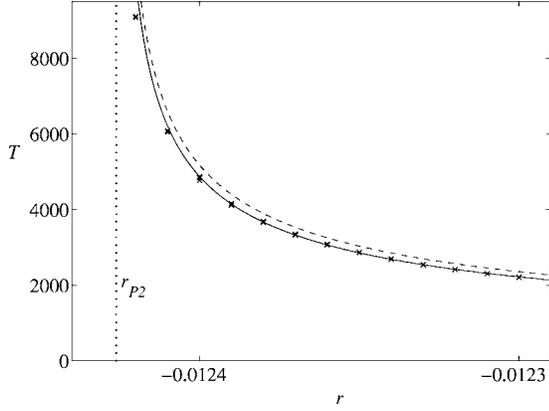
FIG. 15. Transition time to pass by a single saddle node as a function of r for several values near the edge of the pinning region at r_{P2}. At each r, data points from different saddle nodes are closely clustered because the saddle nodes line up at r_{P2}. The solid line is a fit to the data, while the dashed line is the prediction (26).
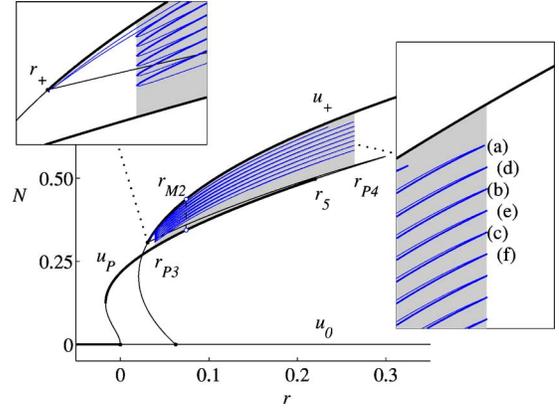

FIG. 16. (Color online) Bifurcation diagram showing the two homoclinic branches biasymptotic to u_+, together with the flat and patterned branches of Fig. 4. Away from the bifurcation at r_+ the homoclinic branches are contained within the pinning region (shaded) between $r_{P3} \simeq 0.038\,74$ and $r_{P4} \simeq 0.2643$. Thick lines indicate stable solutions. For clarity the stability of the localized states is only indicated in the insets, which show the behavior near the saddle nodes. Asymmetric solutions are omitted. The dashed vertical line marks the location of the Maxwell point r_{M2} between the flat and patterned branches. The letters (a)–(f) mark the locations of the profiles shown in Fig. 17.

tion at $r=0$ of the patterned branch from the flat state u_0, and on the other side by the saddle node of the patterned branch at r_3, a regime examined in the context of buckling by Champneys and co-workers [7,8]. Figure 4 shows that another region of bistability is present, lying between r_+ and r_5 where both the flat u_+ branch and the patterned branch are stable. To study this region we shift the origin of r to r_+, and define the quantities $\tilde{u}$ and $\tilde{r}$ as

$$u(x,t) = u_+ - \tilde{u}(x,t), \quad r = r_+ - \tilde{r}.$$

Thus $\tilde{u}$ satisfies the equation

$$\frac{\partial \tilde{u}}{\partial t} = \tilde{r}\left(\frac{2u_{L_c,+}(3gu_{L_c,+} - v)}{q_c^4} - 1\right)\tilde{u} - (\partial_x^2 + q_c^2)^2\tilde{u}$$
$$+ (3gu_{L_c,+} - v)\tilde{u}^2 - g\tilde{u}^3 + O(\tilde{r}^2), \qquad (27)$$

where $u_{L_c,+} = (v + \sqrt{v^2 + 8gq_c^4})/4g \simeq 0.3068$ is the value of u_+ evaluated at r_+. As the $\tilde{u}^2$ coefficient is positive, Eq. (27) is of the same form as the original Eq. (1), and the behavior near r_+ in the new bistable region is mathematically analogous to that described in the preceding section, although this possibility is absent from Refs. [7,8] owing to a different parametrization. In particular, the asymptotic analysis and the computation of the normal form coefficients carried out in Eqs. (12)–(18) and (22) carries over to this case using the transformation

$$u \rightarrow u_+ - u, \qquad (28a)$$

$$r \rightarrow (r_+ - r)\left(\frac{2u_{L_c,+}(3gu_{L_c,+} - v)}{q_c^4} - 1\right), \qquad (28b)$$

$$v \rightarrow 3gu_{L_c,+} - v. \qquad (28c)$$

For example, at $r = r_+$

$$\gamma_3 = \frac{38(3gu_{L_c,+} - v)^2}{9q_c^4} - 3g \simeq 14.6.$$

It follows that this region also contains two branches of homoclinic solutions which, like the patterned branch, bifurcate from the u_+ branch at r_+. As shown in Fig. 16 these homoclinic branches undergo a series of saddle-node bifurcations between r_{P3} and r_{P4}. As in the previous case, there is a Maxwell point r_{M2} within the pinning region where the energy of the flat u_+ branch matches that of the patterned branch. Below this point the patterned state has the lower energy density while above the u_+ state is preferred. However, once again the patterned branch u_P shown in Fig. 16 has a wavelength that does not exactly match the pattern inside the localized states that make up the snakes: near r_5 and r_{P4} the wavelength within the localized states deviates by as much as 15% from L_c. The wavelength discrepancy is most noticeable at large r where the flat state has lower energy density, squeezing the packets so that the observed wavelength within the localized states is less that L_c. It is significant that the patterned branch with this wavelength does *not* undergo a period-doubling bifurcation at r_5. As a result the localized states on the snakes do not inherit the change of stability of u_P at r_5 or indeed any of the bifurcations to nL_c-periodic states that are present near r_5^*, and remain stable all the way up to the saddle node bifurcations at r_{P4}.

As mentioned earlier bifurcations from the u_- branch can be mapped to the u_+ branch. As a result the bistable region that exists between u_- and the patterned branch can be studied within the same framework. The remaining possibility, branches of solutions connecting the u_+ and u_- states, can be excluded on energy grounds: if $v > 0$ ($v < 0$) the energy of
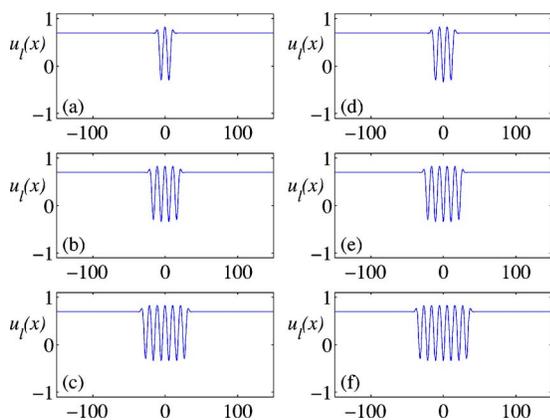
FIG. 17. (Color online) Sample profiles $u_\ell(x)$ at the saddle nodes indicated in Fig. 16. (a)–(c) lie on the $\phi=0$ branch while (d)–(f) lie on the $\phi=\pi$ branch.

the u_+ state is always less than (greater than) the u_- state. Moreover, no pinning is possible. Thus no *stationary* fronts between these two flat states are possible when $v \neq 0$. Kink solutions, present when $v=0$, are discussed in Ref. [8].

IV. LOCALIZED STATES AS A FUNCTION OF v

Thus far we have studied the behavior of Eq. (1) as r varies at fixed values of q_c, v, and g. To explore the v dependence of our results we rescale x and u so that $q_c=0.5$ and $g=1.0$, and vary v. Consider first the bifurcation from the $u=0$ flat state, shown in Fig. 8 at $v=0.41$. Within the normal form (21) changing v corresponds to changing q_2. The condition $q_2=0$ defines a codimension-2 point in the (r,v) plane with coordinates $r=0$, $v=\pm\sqrt{27gq_c^4/38}$; without loss of generality we take $v>0$. At this point $q_4 = 2202g^2/361q_c^6>0$ and the reversible Hopf bifurcation at $r =0$ in Eq. (1) is of the type shown in Fig. 6(b). In this case normal form theory predicts that homoclinic solutions only exist in the subcritical regime $q_2<0$ (i.e., $v^2>27gq_c^4/38$) and only in the range $\mu_D<\mu<0$. The heteroclinic solution at μ_D in the normal form corresponds to the Maxwell point r_{M1} in the partial differential equation. Away from the codimension-2 point we can use the normal form to confirm the existence of homoclinic solutions when $r\lesssim0$ and it is these small amplitude solutions that provide a starting point for the numerical continuation to large amplitude used to determine the extent of the pinning region. We can also follow the Maxwell point.

Figure 18 summarizes the regions of existence of heteroclinic connections to the trivial flat state u_0. In view of the parameter symmetry $(u,v)\to(-u,-v)$ of Eq. (1) a mirror image of this picture exists in the $v<0$ region of parameter space. The bifurcation diagram in Fig. 8 corresponds to a horizontal slice through this figure at $v=0.41$ and is typical of the behavior below $v\simeq0.688$. Above this value of v a new Maxwell point, corresponding to equal energies of the u_0 and u_+ states,

$$r_{M3} = q_c^4 - \frac{2v^2}{9g}, \qquad (29)$$

becomes dynamically important. For $v>\sqrt{9gq_c^4/2}$ this Maxwell point lies to the right of the bifurcation at r_+, within the
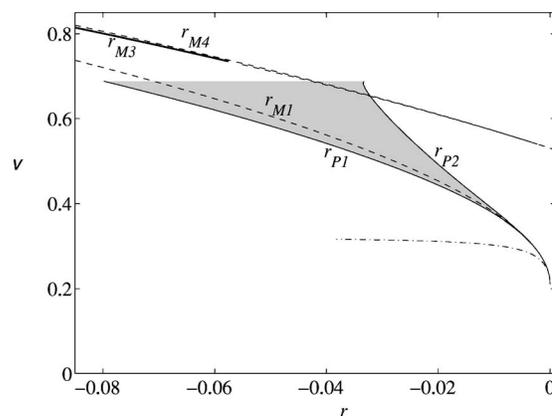

FIG. 18. The pinning region (shaded) of solutions heteroclinic to the trivial u_0 state. This region, located between r_{P1} and r_{P2}, is created in a codimension-2 bifurcation at $(r,v)\simeq(0,0.2107)$. Dashed lines correspond to the Maxwell points r_{M1}, r_{M3}, and r_{M4}. The thick solid line corresponds to homoclinic snaking of the type shown in Fig. 19. The dash-dotted line marks the location of the heteroclinic orbits (Maxwell points) as predicted by the normal form.

region where u_+ is stable, and at $v\simeq0.688$ $r_{M3}=r_{P2}$. Thus for $v\gtrsim0.688$ (i.e., above the horizontal boundary of the shaded region in Fig. 18) the new Maxwell point enters the pinning region around r_{M1} and the structure of the flat and patterned states changes, as do the homoclinic branches. In particular, above $v\simeq0.735$ the $\phi=0,\pi$ homoclinic branches created at the origin undergo homoclinic snaking towards the u_+ state instead of u_P. Since u_+ is a spatially homogeneous state no pinning occurs, and the snakes collapse asymptotically to a single point at $r=r_{M3}$. Thus at r_{M3} an infinite number of homoclinic states of different lengths biasymptotic to u_0 is still present, but away from r_{M3} only a finite number of such states remains [23]. Bifurcation diagrams describing these homoclinic states for $\phi=0,\pi$ are shown in Fig. 19. The solutions on the $\phi=\pi$ branch, shown in Fig. 19(b), include a small region of width of order L_c where the solution profile dips back down to $u\sim0$ in order that $x=0$ remains a minimum.

Between $v\sim0.688$ and $v\sim0.735$ there is a transition region as the homoclinic snaking in the pinning region around r_{M1} (Fig. 8) shifts to straddle the new heteroclinic connection at r_{M3} (Fig. 19). This intermediate region (Fig. 20) is complicated by the existence of yet another new Maxwell point, labeled r_{M4}, between u_0 and the *unstable* section of the patterned branch near r_+. This Maxwell point is close to r_{M3} because near r_+ the energies of the flat and patterned states are very similar. The profiles along both the $\phi=0$ and $\phi=\pi$ branches contain domains within which $u(x)$ resembles three different states: u_0, the (unstable) solution from the upper segment of the patterned branch, and the (stable) solution from the middle segment. As one proceeds up each branch the fronts between the flat and unstable pattern move apart filling most of the domain with the unstable pattern. However, the fronts between the two structured states remain fixed leaving a small patch of the stable pattern near the origin. It is this "double" structure that is responsible for the complex structure of the corresponding snakes, cf. Ref. [24].
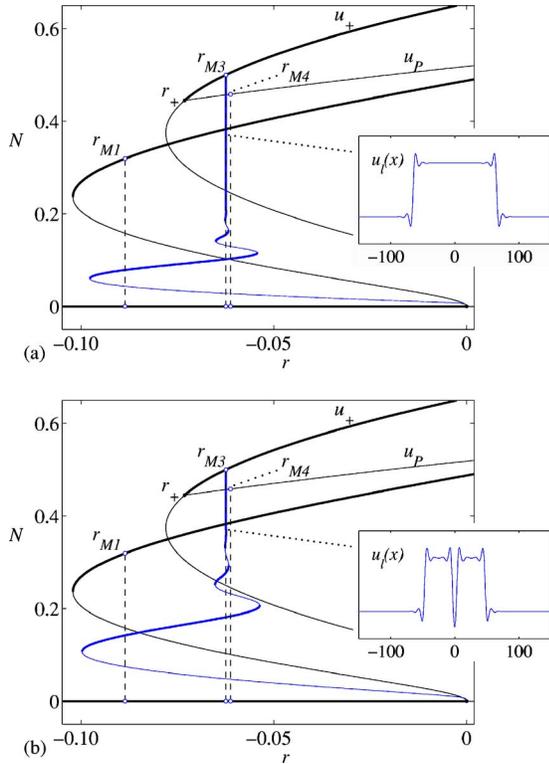
FIG. 19. (Color online) Bifurcation diagram corresponding to a horizontal slice through Fig. 18 at $v=0.75$ illustrating (a) $\phi=0$ and (b) $\phi=\pi$ homoclinic snaking around a heteroclinic connection between the two flat states u_0 and u_+. Thick lines indicate stable solutions; asymmetric states are omitted. The insets show typical solution profiles as the envelope widens and fills with the u_+ state.

Note in particular the unusual looping on the lower part of the $\phi=0$ branch (absent from the $\phi=\pi$ branch) whose origin remains unclear. An analysis of the eigenvalues shows that all such states far up the snaking branches are unstable.

The snaking shown in Fig. 20 is a consequence of the Maxwell point r_{M4} but two other Maxwell points are present as well. Snaking about the latter is illustrated in Figs. 16 and 19. It is natural to ask what selects the Maxwell point about which a snake develops, and if snakes abandon one Maxwell point in favor of another as parameters are varied how such transitions take place. For example, Fig. 18 suggests an abrupt end to the pinning region surrounding r_{M1} at $v \simeq 0.688$ that may mark a genuine limit point above which the snaking branch transitions to one of the other Maxwell points. One may think that only a single Maxwell point can be graced by snakes since only a single pair of localized states ever bifurcates from the flat state. Whether snakes can split at finite amplitude into multiple pairs remains unclear. Moreover, as discussed further below, snaking does not even require the presence of Maxwell points.

We next consider homoclinic states biasymptotic to u_+. It is easy to show using Eq. (28) that at r_+ the coefficient $q_2 <0$ for all values of v. Hence this bifurcation is always subcritical and no codimension-2 point occurs from which heteroclinic states can be traced. Small amplitude homoclinic solutions near r_+ remain, however, and are given by Eqs. (18) and (28). These can be followed numerically to larger
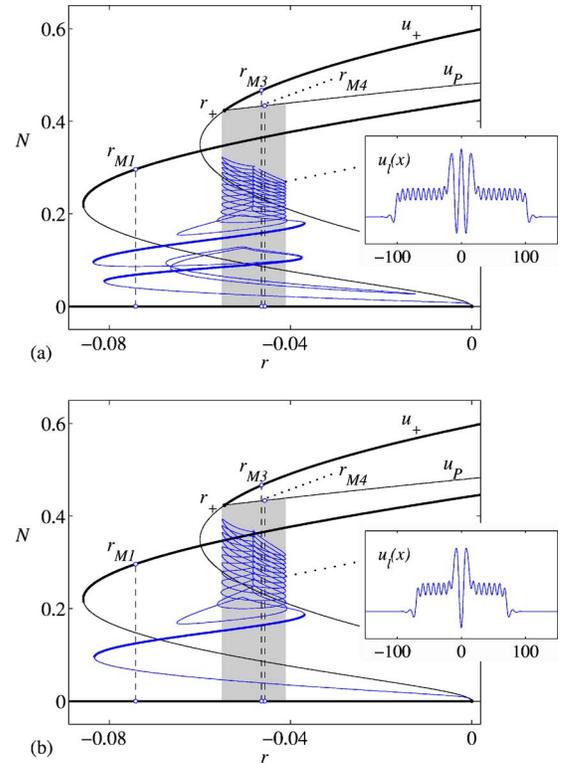
FIG. 20. (Color online) Bifurcation diagram corresponding to a horizontal slice through Fig. 18 at $v=0.70$. In (a) the localized states correspond to $\phi=0$ while (b) shows the $\phi=\pi$ branch. Thick lines indicate stable solutions; asymmetric states are omitted. The insets show typical solution profiles far up the snaking branches. The larger (smaller) amplitude states correspond to the stable middle (unstable upper) segments of the u_P branch.

amplitude. Figure 21 shows the location in (r,v) phase space of the pinning region that contains solutions heteroclinic to u_+. At each point within this region there exists an infinite number of homoclinic solutions that differ only in width. We identify three possible structures that describe the organization of these states along one-parameter slices through this figure. The first is regular homoclinic snaking, shown previously in Fig. 16, with all states joined into a finite number of branches according to the phase ϕ (here $\phi=0,\pi$). The second possibility may be termed *semi-infinite snaking* and arises when one of the lines of saddle nodes moves off to infinity. The third case, which we call *homoclinic loops*, consists of an infinite stack of disconnected isolas, each made up of solutions with a fixed number of oscillations; this number increases from isola to isola as one moves up the stack.

Constant v slices of Fig. 21 indicate that both Figs. 4 and 16 are incomplete. In each case the complete picture resembles that shown in Fig. 22 but includes an extra stack of disconnected patterned states that extend to arbitrarily large r and form what we have called a semi-infinite snake. It is interesting that the latter is not associated with a Maxwell point: the only Maxwell point between the flat and patterned states occurs at r_{M2} in the regular homoclinic snaking region. Both the regular and semi-infinite snaking regions apparently persist to arbitrarily large v.

Close inspection of Fig. 22 shows that the pinning region
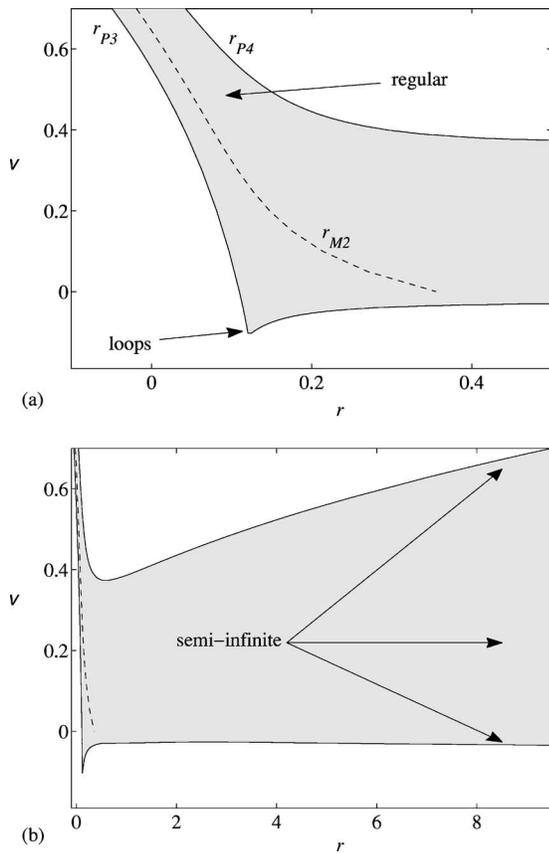
FIG. 21. (a) The pinning region (shaded) of solutions heteroclinic to the u_+ state. (b) The same but on a larger scale.

extends *beyond* the patterned branches. This is a consequence of the wavelength selection mentioned above. The patterned branch shown in the figure has wavelength L_c; at large r this wavelength differs from that within the localized state. Inspection of the wave number of the pattern within these states shows that the preferred value is about 30% higher. The patterned branch corresponding to this wave
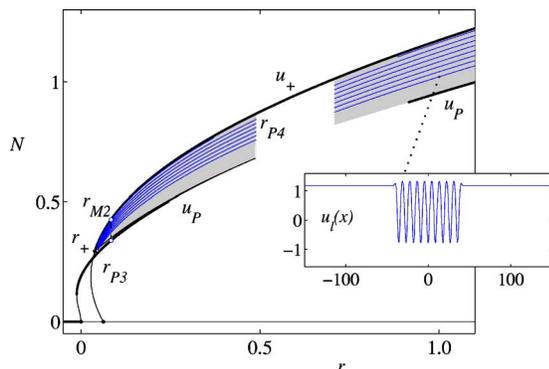

FIG. 22. (Color online) Bifurcation diagram corresponding to a horizontal slice through Fig. 21 at $v=0.375$. Asymmetric states are omitted. The depinning transitions for the finite snaking region occur at $r_{P3} \simeq 0.046\,96$ and $r_{P4} \simeq 0.4891$, and for the semi-infinite snaking region at $r \simeq 0.7077$. The only Maxwell point between the u_+ and patterned branches (r_{M2}) occurs within the finite snaking region.
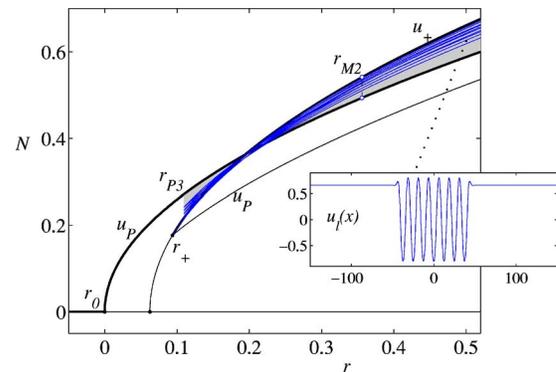

FIG. 23. (Color online) Bifurcation diagram corresponding to a horizontal slice through Fig. 21 at $v=0$. Asymmetric states are omitted. The depinning transition occurs at $r_{P3} \simeq 0.109\,73$ and the Maxwell point is at $r_{M2} \simeq 0.355$. The apparent branch crossings near $r \sim 0.2$ are an artifact of the norm plotted on the vertical axis.

number extends all the way back to the pinning transition, providing support for all the localized states in the semi-infinite snaking region.

As v decreases below $v \simeq 0.3733$ the states in Fig. 22 merge in a "zipping" transition [25], leaving a single semi-infinite snake that extends from r_{P3} to $r=\infty$. It is remarkable that this region includes the case $v=0$ corresponding to the standard Swift-Hohenberg equation with no quadratic nonlinearity. The corresponding bifurcation diagram is shown in Fig. 23 and is typical of this region. The case $v=0$ has been studied in the past (e.g., Refs. [22,26]) but the disconnected branches of (stable) localized states have not been noted before. Indeed, in view of the general scaling $r \sim q_c^4$ we find that $r_{P3} = 0.109\,73 = 1.756 q_c^4$ at $v=0$, a prediction that agrees with the location of the depinning transition found in Ref. [22] ($r \simeq 1.74$, $q_c=1$). Likewise the Maxwell point occurs at $r_{M2} = 0.355 = 5.68 q_c^4$, as found in Ref. [27].

Below $v \lesssim -0.03$ the semi-infinite snake "unzips" into two segments in r, one finite and one extending to $r=\infty$. In the finite segment the bifurcation diagrams (Fig. 24) are now topologically distinct from those in Fig. 22, consisting of stacks of homoclinic isolas instead of snakes. Each isola contains a segment with stable localized states. At these values of v the two branches of patterned solutions created at r_0 and r_+ extend to infinite r, and the semi-infinite snaking region does contain a Maxwell point where the flat and patterned states have equal energies. However, the isola region possesses no such point. Further decrease below $v \simeq -0.109$ causes the homoclinic isolas to shrink and vanish, but the semi-infinite snaking region remains at arbitrarily large negative v.

At first glance the two different regions of homoclinic snaking identified in the previous section (one created at r_0 and shown in Fig. 8 and the other at r_+ and shown in Fig. 16) appear similar but despite the mathematical similarity between the bifurcations at r_0 and r_+ this is not the case. The saddle node at r_4 is created when stable and unstable branches of patterned solutions pinch off and disconnect, in contrast to what happens at r_3. Thus the semi-infinite snakes are likely inherited from snakes that are ultimately associated with Maxwell points at smaller values of r. There is no ana-
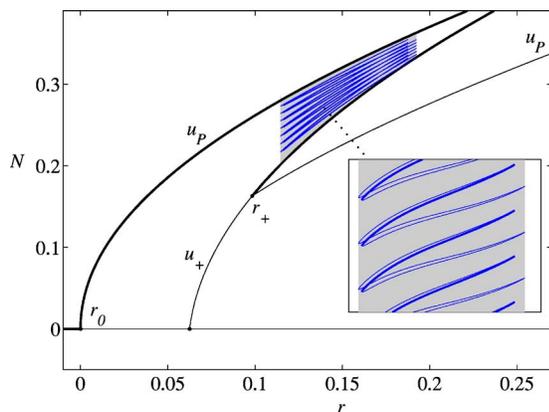
FIG. 24. (Color online) Bifurcation diagram corresponding to a horizontal slice through Fig. 21 at $v = -0.057$. Asymmetric states are omitted. The inset shows isolas of localized states that fill the pinning region and account for the term "homoclinic isolas." Each isola corresponds to solutions with the same number of oscillations of the pattern. Thick lines indicate stability. There is also a semi-infinite snaking region at this v value but it is omitted from the figure because it only exists at very large r.

log of this behavior for the first snake, consisting of localized states biasymptotic to $u_0 = 0$ (cf. Fig. 18). This difference is a consequence of terms such as ru^2 and r^2u that are present in Eq. (27) for $\tilde{u}$ but not in Eq. (1).

V. DISCUSSION AND CONCLUSIONS

In this paper we have revisited the generalized Swift-Hohenberg equation, and reexamined the formation of spatially localized states within this system. We have focused on the relation between finite amplitude localized states and the small amplitude localized states that can be computed via perturbation theory. In addition we have examined the linear stability of these states. We have shown that a pair of branches of localized states generically bifurcates from the trivial state as the bifurcation parameter r increases. Both bifurcations are subcritical. The solutions on these two branches are reflection symmetric and differ only in their phase $\phi = 0, \pi$. Initially both branches are unstable, but with increasing $|r|$ begin to "snake" in a characteristic fashion as the localized state broadens, and begins to approach a spatially periodic state. The snaking generates a sequence of saddle-node bifurcations at each of which the pattern adds a pair of "rolls." These bifurcations accumulate rapidly, with the interval between the limit points defining the so-called "pinning" region. We have seen that the pinning region is a consequence of locking of the fronts at either end of the localized structure to the underlying periodic state, and as such can be thought of as a broadened Maxwell point. Each pinning region contains an infinite number of stable localized states of both phases.

To obtain these results we formulated the problem of finding localized states as a problem of finding homoclinic orbits in a fourth order dynamical system in space. The reversible structure of this system is responsible for the presence of 1:1 reversible Hopf bifurcations at particular values of r, and the

theory of this bifurcation provides a key to understanding the origin of the localized states. This theory requires the use of beyond-all-orders asymptotics [13,14,28]; for this reason the phase selection between the $\phi = 0$ and $\phi = \pi$ branches is initially extremely weak, as is the amplitude of the snake. Both processes only become significant in the pinning region. High up each snake the localized states become broad and begin to resemble heteroclinic orbits, i.e., slugs of a periodic wavetrain embedded in a flat background.

We have seen that the generalized Swift-Hohenberg equation admits multiple Maxwell points, and hence multiple pinning regions exhibiting snaking. We have focused on three such regions. The first, present for $r < 0$, occurs when the trivial and patterned states have equal energies. The second and third arise when the patterned state has the same energy as the nontrivial flat states $u_\pm$. The corresponding pinning regions describe the location of localized states that are bi-asymptotic to a nonzero flat state. In other regimes we have located infinite stacks of isolas of localized states. However, perhaps the most unexpected observation is that there is a broad range of values of v for which stacks of localized states come in from infinity (in r), turn around in a saddle-node bifurcation, and return to infinity. These states are highly nonlinear, acquire stability at the saddle-node bifurcations, and are present even when $v = 0$, i.e., in the usual Swift-Hohenberg equation with only a single stabilizing cubic nonlinearity. Throughout the paper we have only considered the so-called single pulse solutions. Multipulse solutions, consisting of several more or less isolated localized states interacting via their tails, possess rich behavior in their own right [14,21,28], but are beyond the scope of the present work.

Localized states are of course of great interest to pattern formation. They occur not only in vibrating granular media [29] and polymeric fluids [30], but also in reaction-diffusion systems [9], nonlinear optics [31–33], ferrofluids in a magnetic field [34], neuronal networks [35], and in several convection systems [36–42]. They are also present in the Swift-Hohenberg equation with cubic and quintic nonlinearities [20,43]. Two-dimensional localized patterns also exhibit snaking [6,33,44]. In particular, the theory of localized buckling of long struts bears a substantial similarity to the work reported above [7,8]. This in turn is closely related to the study of solitary waves in the fifth order Korteweg–de Vries (KdV) equation arising in the theory of long wavelength water waves [45,46] and related systems [47]. In particular the solitary waves studied in the context of the fifth order KdV equation correspond precisely to the localized states of the Swift-Hohenberg equation (1) in the special case $g = 0$, with the parameter r related to the speed of the waves. Indeed, it is in this context that the bifurcation of the $\phi = 0, \pi$ branches of localized states from the trivial state was first established [48], the dominant nonlinearity near $r = 0$ being quadratic. Moreover, no *other* branches of localized states bifurcate from $r = 0$ [14]. It is worth mentioning that the water wave problem, like the buckling problem, is fundamentally time independent. Thus the question of linearized stability does not arise in a natural way, unless additional physical notions such as wave radiation to infinity are included. It is for this reason that stability questions have not been central to the

study of localized states in great many cases, although in other contexts the stability of the solutions along the snakes has been studied [33,49] albeit with respect to symmetric perturbations only.

It is worth mentioning that in the large body of work on localized buckling the load parameter enters as the coefficient of the second derivative. Thus in this class of problems the parameter that is varied is the wave number q_c, while keeping a particular combination of r and q_c^4 constant. This procedure represents a distinct cut through the parameter plane that encounters only one of the possible Maxwell points, corresponding to our first snaking region (near $r=0$). We surmise that this is the reason why the interesting behavior in and near the other snaking regions described here has not already been noted.

[1] S. Fauve and O. Thual, Phys. Rev. Lett. **64**, 282 (1990).

[2] K. Kirchgässner, J. Differ. Equations **45**, 113 (1982).

[3] G. Iooss and M. C. Perouème, J. Differ. Equations **102**, 62 (1993).

[4] Y. Pomeau, Physica D **23**, 3 (1986).

[5] M. F. Hilali, S. Métens, P. Borckmans, and G. Dewel, Phys. Rev. E **51**, 2046 (1995).

[6] P. Coullet, C. Riera, and C. Tresser, Phys. Rev. Lett. **84**, 3069 (2000).

[7] A. R. Champneys, Physica D **112**, 158 (1998).

[8] G. W. Hunt, M. A. Peletier, A. R. Champneys, P. D. Woods, M. Ahmer Wadee, C. J. Budd, and G. J. Lord, Nonlinear Dyn. **21**, 3 (2000).

[9] Y. Nishiura and D. Ueyama, Physica D **130**, 73 (1999).

[10] E. Doedel, R. C. Paffenroth, A. R. Champneys, T. F. Fairgrieve, Y. A. Kuznetsov, B. E. Oldeman, B. Sandstede, and X. Wang, AUTO97: Continuation and bifurcation software for ordinary differential equations, Concordia University (2002) http://indy.cs.concordia.ca/auto/main.html

[11] U. Thiele and E. Knobloch, Physica D **190**, 213 (2004).

[12] More precisely, no localized states with exponential approach to $u_0=0$ are possible when $r>0$.

[13] D. Bensimon, B. I. Shraiman, and V. Croquette, Phys. Rev. A **38**, 5461 (1988).

[14] T.-S. Yang and T. R. Akylas, J. Fluid Mech. **330**, 215 (1997).

[15] I. Melbourne, J. Nonlinear Sci. **8**, 1 (1998).

[16] More generally the terms beyond all orders select an even number of fixed points, but the additional localized states cannot bifurcate from $r=0$.

[17] B. Sandstede, Philos. Trans. R. Soc. London, Ser. A **355**, 2083 (1997).

[18] These coefficients disagree with those given by P. D. Woods and A. R. Champneys, Physica D **129**, 147 (1999).

[19] C. J. Budd and R. Kuske, Physica D **208**, 73 (2005).

[20] J. Burke and E. Knobloch (unpublished).

[21] P. Coullet, C. Riera, and C. Tresser, Chaos **14**, 193 (2004).

[22] I. S. Aranson, B. A. Malomed, L. M. Pismen, and L. S. Tsimring, Phys. Rev. E **62**, R5 (2000).

[23] J. Knobloch and T. Wagenknecht, Physica D **206**, 82 (2005).

[24] D. Gomila, A. J. Scroggie, and W. J. Firth (unpublished).

[25] G. H. M. van der Heijden, Dyn. Syst. **15**, 159 (2000).

[26] L. A. Peletier and W. C. Troy, *Spatial Patterns: Higher Order Models in Physics and Mechanics* (Birkhäuser, Boston, 2001).

[27] A. Hagberg, A. Yochelis, H. Yizhaq, C. Elphick, L. Pismen, and E. Meron, Physica D **217**, 186 (2006).

[28] M. K. Wadee, C. D. Coman, and A. P. Bassom, Physica D **163**, 26 (2002).

[29] P. B. Umbanhowar, F. Melo, and H. L. Swinney, Nature (London) **382**, 793 (1996).

[30] O. Lioubashevski, Y. Hamiel, A. Agnon, Z. Reches, and J. Fineberg, Phys. Rev. Lett. **83**, 3190 (1999).

[31] M. Tlidi, P. Mandel, and R. Lefever, Phys. Rev. Lett. **73**, 640 (1994).

[32] A. G. Vladimirov, J. M. McSloy, D. V. Skryabin, and W. J. Firth, Phys. Rev. E **65**, 046606 (2002).

[33] J. M. McSloy, W. J. Firth, G. K. Harkness, and G.-L. Oppo, Phys. Rev. E **66**, 046606 (2002).

[34] R. Richter and I. V. Barashenkov, Phys. Rev. Lett. **94**, 184503 (2005).

[35] C. R. Laing, W. C. Troy, B. Gutkin, and G. B. Ermentrout, SIAM J. Appl. Math. **63**, 62 (2002).

[36] A. Spina, J. Toomre, and E. Knobloch, Phys. Rev. E **57**, 524 (1998).

[37] S. Blanchflower, Phys. Lett. A **261**, 74 (1999).

[38] S. Blanchflower and N. O. Weiss, Phys. Lett. A **294**, 297 (2002).

[39] O. Batiste and E. Knobloch, Phys. Fluids **17**, 064102 (2005).

[40] O. Batiste and E. Knobloch, Phys. Rev. Lett. **95**, 244501 (2005).

[41] O. Batiste, E. Knobloch, A. Alonso, and I. Mercader J. Fluid Mech (to be published).

[42] J. H. P. Dawes (unpublished).

[43] H. Sakaguchi and H. Brand, Physica D **97**, 274 (1996).

[44] D. Lloyd, Ph.D. thesis, University of Bristol, Bristol.

[45] A. R. Champneys and J. F. Toland, Nonlinearity **6**, 665 (1993).

[46] B. Buffoni, A. R. Champneys, and J. F. Toland, J. Dyn. Differ. Equ. **8**, 221 (1996).

[47] A. R. Champneys, M. D. Groves, and P. D. Woods, Phys. Lett. A **271**, 178 (2000).

[48] R. Grimshaw, B. Malomed, and E. Benilov, Physica D **77**, 473 (1994).

[49] I. V. Barashenkov, S. Cross, and B. A. Malomed, Phys. Rev. E **68**, 056605 (2003).